J. Acoust. Soc. Jpn. (*E*) **8**, 5 (1987)

Selective detection of second harmonic sound generated at the focal region in a finite amplitude focusing field

Shigemi Saito and Bong Chae Kim

Faculty of Marine Science and Technology, Tokai University, 3–20–1, Orido, Shimizu, 424 Japan

(*Received 14 January 1987*)

A method for selective detection of the second harmonic component generated at the focal region in a focused sound field due to the local nonlinear properties of medium is discussed. The phase shift of sound waves passing through the focus offers the principle of the present method. Assuming a source with a Gaussian profile excitation to avoid the edge diffraction, the effect of an inserted sample with a nonlinearity parameter different from that of surrounding liquid (water) is theoretically analyzed. The experiment employing a sample of benzyl alcohol shows the validity of the theory. The quadrature component of the second harmonic which differs in phase by $\pi/2$ radians from that of non-diffraction case corresponds well to the second harmonic generation at the focus, i.e. the nonlinear property of the sample within the focal region.

PACS number: 43. 25. Cb, 43. 25. Jh, 43. 35. Sx

LIST OF SYMBOLS

a: source radius
A: constant associated with Gaussian distribution
B/A: parameter of nonlinearity
c_0: sound speed
D: focal length
$E_1(\cdot)$: exponential integral
j: $\sqrt{-1}$
$J_0(\cdot)$: Bessel function of order 0
k: fundamental wavenumber
L: thickness of inserted sample
P: power of second harmonic sound
q_1: fundamental velocity potential parameter
q_{10}: amplitude of ϕ_1
q_2: second harmonic velocity potential parameter
q_{20}: amplitude of ϕ_2
$Q_s, \bar{Q}_s$: values associated with quadrature component of the second harmonic
$Q_c, \bar{Q}_c$: values associated with inphase component of the second harmonic
r: radial coordinate
R: function associated with r dependence of fundamental amplitude
s: Hankel transform variable
t: time variable
u_0: amplitude of the source velocity at $r=0$
$u(r)$: amplitude of the source velocity
x, y: variables of integration
z: axial coordinate
z_L: axial coordinate of the center of sample
$\Delta z_{1/e}$: focal region length
β: parameter of nonlinearity
β_L: parameter of nonlinearity of inserted sample
θ: phase parameter ($=\theta_2-2\theta_1$)
$\bar{\theta}$: phase parameter of the pressure averaged on surface
θ_1: phase of q_1
θ_2: phase of q_2
ξ: integral variable
π: 3.14159 . .

ρ: ambient density
σ: shock parameter
ϕ: total velocity potential
ϕ_1: fundamental velocity potential
ϕ_2: second harmonic velocity potential
ω: fundamental angular frequency

1. INTRODUCTION

It is well known that an intense sound produces higher harmonics with propagation caused by nonlinear distortion. Since the largest part of the distortion is due to an elastic nonlinearity of medium where pressure is not in linear proportion to density, a parameter of nonlinearity B/A denoting this characteristic is widely used for characterizing materials and substances. Another parameter of nonlinearity β $(=1+B/2A)$ describing the dependence of local sound speed on particle velocity is treated here.

The thermodynamic method and finite-amplitude method are most commonly used to measure the parameter of nonlinearity of medium.[1,2] Recently, some new methods to visualize the inhomogeneity of the nonlinear properties in biological tissues, utilizing the principle that a weak probe wave suffers a phase modulation due to the nonlinear interaction with an overlapping pumping wave of high intensity, was proposed and developed.[3-6]

A spherical focusing source is generally used to increase the resolution in applications such as ultrasonic diagnosis and acoustic microscopy. In this focusing field, high frequency and strong focusing effect accelerate the nonlinear distortion of sound.[7] It has already been suggested that one can record the nonlinear properties of an object immersed in the focal region by detecting a second harmonic component in acoustic microscopes.[8] However a subsequent article gave the concluding remarks that the nonlinear characteristic of thin samples could be hardly detected through the second harmonic signal, because the greatest part of the second harmonic observed in a microscope was assumed to be generated outside the sample.[9] Fairly complicated microscopes were then proposed, and developed to enhance the nonlinear distortion due to the sample[10,11]; however it seems that little progress have been made so far.

On the second harmonic component nonlinearly generated at a focused sound field in homogeneous media, Lucas and Muir[12,13] offered an analytical model taking diffraction effects into account, and the present authors *et al.*[14] and Humphrey *et al.*[15] showed a good agreement between the theory and experiment. Through the comparison of theory and experiment, the present authors *et al.* proved that the second harmonic observed in the post focal region was generated almost at the focal region. They also suggested that the second harmonic sounds generated at the pre and post focal regions suffered destructive interference (or cancellation) in the post focal region because of π radian phase shift when passing through the focus. This makes the second harmonic sound generated at the focal region be dominant at the post focal region. An increased resolution of the acoustic microscope working at very high intensity level, which may be explained by the aforementioned cancellation, has already been reported.[16] These phenomena appear to differ from the concluding remarks of Ref. 9). Therefore the possibility of detecting the nonlinear characteristic of an inserted sample within a conventional acoustic microscope needs to be examined again.

The present paper presents a theoretical prediction of the behavior of the second harmonic component generated at focusing fields with a sample inserted within the focal region. Validity of the theory is experimentally demonstrated by detecting the component due to the nonlinearity of the inserted sample within a focal region.

2. THEORETICAL PREDICTION

2.1 Behavior of Focusing Field

The sound field formed by a uniformly excited spherically concave focusing source is rather complicated on the symmetrical axis due to the source edge diffraction. On the other hand, the sound amplitude distribution is rather simplified except in the vicinity of the axis, as is the distribution of a phase parameter.[14] In order to examine typical fields peculiar to spherically focusing sounds, the source amplitude is assumed to have a Gaussian distribution without an edge of source, where an edge diffraction effect may not occur to complicate the on-axis field. We suppose a focusing source with the focal length D located in cylindrical coordinates as illustrated in Fig. 1. A sinusoidal sound wave with the angular frequency ω and the wavenumber k is radiated in water. The velocity potential of a fundamental component

$$\phi_1(r, z)=q_1(r, z)\exp\{j(kz-\omega t)\} \quad (1)$$

is given by solving a following equation.

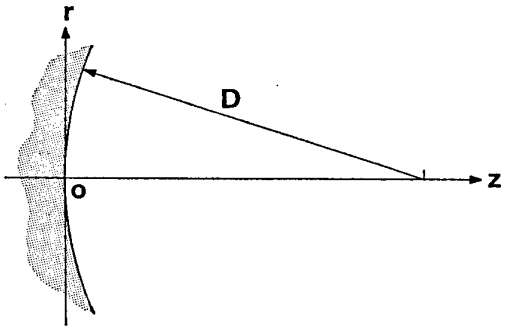

Fig. 1 Geometry and notation.

$$\frac{1}{r}\frac{\partial}{\partial r}\left(r\frac{\partial q_1}{\partial r}\right)+\frac{\partial^2 q_1}{\partial z^2}+2jk\frac{\partial q_1}{\partial z}=0. \qquad (2)$$

A boundary condition implying a Gaussian envelope excitation can be replaced by the condition approximated on the plane $z=0$ as follows:

$$q_1(r,0)=\frac{u_0}{jk}\exp\left\{-\left(A+j\frac{k}{2D}\right)r^2\right\}, \qquad (3)$$

where A corresponds the inverse of variance of the Gaussian distribution, and u_0 is the source velocity at $r=0$. This approximation is valid, provided the restriction $1\ll k/\sqrt{A}\ll 16\pi(D\sqrt{A})^3$ is satisfied. Applying a Hankel transform

$$\tilde{q}_1(s,z)=\int_0^\infty q_1(r,z)J_0(sr)rdr \qquad (4)$$

to both sides of Eq. (2), the equation reduces to

$$-s^2\tilde{q}_1+\frac{d^2\tilde{q}_1}{dz^2}+2jk\frac{d\tilde{q}_1}{dz}=0 \qquad (5)$$

where $J_0(\cdot)$ is the zero order Bessel function. The solution of this equation is

$$\tilde{q}_1(s,z)=\tilde{q}_1(s,0)\exp\{j[\sqrt{k^2-s^2}-k]z\}. \qquad (6)$$

A Fresnel approximation valid at fairly low concavity, e.g. $D\sqrt{a}\gtrsim 3$, simplifies the solution to be

$$\tilde{q}_1(s,z)=\tilde{q}_1(s,0)\exp\left(-j\frac{s^2z}{2k}\right). \qquad (7)$$

Here $\tilde{q}_1(s,0)$ is the Hankel transform of Eq. (3), that is

$$\tilde{q}_1(s,0)=\frac{u_0}{jk}\int_0^\infty \exp\left\{-\left(A+j\frac{k}{2D}\right)r^2\right\}J_0(sr)rdr. \qquad (8)$$

The use of integral formula[17]

$$\int_0^\infty x\exp(-ax^2)J_0(bx)dx=\frac{1}{2a}\exp\left(-\frac{b^2}{4a}\right) \quad (\mathrm{Re}\ a>0) \qquad (9)$$

and the inverse Hankel transform

$$q_1(r,z)=\int_0^\infty \tilde{q}_1(s,z)J_0(rs)sds \qquad (10)$$

leads the solution of the fundamental component as

$$q_1(r,z)=\frac{u_0}{j2k\left(A+j\frac{k}{2D}\right)}\int_0^\infty \cdot\exp\left\{-\frac{s^2}{4\left(A+j\frac{k}{2D}\right)}\right\} \cdot\exp\left(-j\frac{s^2z}{2k}\right)J_0(rs)sds. \qquad (11)$$

Using the integral formula again, one obtains the expression

$$q_1=q_{10}\exp(j\theta_1)=-\frac{u_0}{g(z)z}\exp\left[j\frac{kr^2}{2z}\left(1+\frac{jk}{g(z)z}\right)\right], \qquad (12)$$

where $g(z)=2A-jk(1/z-1/D)$.

The velocity potential of a nonlinearly generated second harmonic component

$$\phi_2(r,z)=q_2(r,z)\exp\{j2(kz-\omega t)\} \qquad (13)$$

can be given by the perturbation solution of Lighthill's equation. The Lighthill equation

$$\frac{1}{r}\frac{\partial}{\partial r}\left(r\frac{\partial q_2}{\partial r}\right)+\frac{\partial^2 q_2}{\partial z^2}+4jk\frac{\partial q_2}{\partial z}=j\frac{\beta k^3}{c_0}q_1^2 \qquad (14)$$

has been linearlized by substituting the above solution q_1 into the inhomogeneous term. Here c_0 is the sound speed, and β is the parameter of nonlinearity of water. The boundary condition

$$q_2(r,0)=0 \qquad (15)$$

is imposed on Eq. (14). Employing the Hankel transform, the Fresnel approximation and the integral formula similarly as in obtaining q_1, one finally derives the solution of a second harmonic component as follows:

$$q_2=q_{20}\exp(j\theta_2)=\frac{\beta k^2u_0^2}{4c_0g(z)z}\exp\left[j\frac{kr^2}{z}\left(1+\frac{jk}{g(z)z}\right)\right]\int_0^z\frac{dz'}{g(z')z'}=\frac{\beta k^2u_0^2}{4c_0\left(2A+j\frac{k}{D}\right)g(z)z}\exp\left[j\frac{kr^2}{z}\left(1+\frac{jk}{g(z)z}\right)\right] \cdot\left[\log\left|\frac{g(z)z}{k}\right|+j\left(\tan^{-1}\left(\frac{2A}{k}\left(1+\frac{k^2}{4A^2D^2}\right)z-\frac{k}{2AD}\right)+\tan^{-1}\left(\frac{k}{2AD}\right)\right)\right]. \qquad (16)$$

The total velocity potential ϕ neglecting all harmonics higher than the second is supposed to be a sum of the velocity potentials of the fundamental component and second harmonic component, that is

$$\begin{aligned}\phi&=\phi_1+\phi_2\\&=q_{10}[\exp\{j(kz-\omega t+\theta_1)\}\\&\quad+(Q_c+jQ_s)\exp\{j2(kz-\omega t+\theta_1)\}]\end{aligned}\tag{17}$$

where $Q_c=(q_{20}/q_{10})\cos\theta$, $Q_s=(q_{20}/q_{10})\sin\theta$, and $\theta=\theta_2-2\theta_1$. A waveform of this sound then obviously depends on the phase parameter θ as well as on the value of q_{20}/q_{10}.

The parameters of the source in water employed for a standard model are $f=2.0$ MHz, $D=85$ mm and $A=1{,}250\ \mathrm{m}^{-2}$. The numerical computation results of q_{10}, θ_1, q_{20} and θ along the symmetrical axis ($r=0$) using Eqs. (12) and (16) are shown in Figs. 2 and 3. Both quantities q_{10} and q_{20} attain maximum values at $z=D$ showing that the radiated sound focuses in the focal point. The phase θ_1 rapidly varies within the range $D-\Delta z_{1/e}/2<z<D+\Delta z_{1/e}/2$, and finally the fundamental component advances by π radians in phase. Here $\Delta z_{1/e}$, a distance between two axial points of $1/e$ amplitude, is taken to represent the focal region length measured on the z axis. In the case of a Gaussian source, this is given by a relation

$$\Delta z_{1/e}\doteqdot\frac{10AD^2}{k},\tag{18}$$

and accordingly $\Delta z_{1/e}=11$ mm in the present standard model. Since the second harmonic component generated in the pre-focal region also undergoes π radian phase shift, this component is opposite in phase to that newly generated in the post focal region. After the propagation to some range in the post focal region, the second harmonic component generated in the pre-focal region is expected to disappear because of destructive interference. In particular here, the value of θ must be $\pi/2$ radians to yield that $Q_c=0$, and a surviving second harmonic component generated in the region outside the pre and post focal regions, namely in the focal region, is expected to be detected.

Figure 4 shows the power of the second harmonic sound transmitting through a plane perpendicular to the z axis to be

$$P(z)=\frac{4\pi\rho\omega^2}{c_0}\int_0^\infty r|q_2|^2dr,\tag{19}$$

which can be evaluated in terms of q_2 in Eq. (16), where ρ is the ambient density. The power which attains a maximum on the focal plane becomes small in the post focal region due to the destructive interference. Since the component whose phase parameter θ is $\pi/2$ is not cancelled, the power of this component survives even at $z=2D$.

One can see that the dependence of the quantity q_{10} on the radial distance r is expressed by the function $\exp[-A(kr/z|g(z)|)^2]$ ($\equiv R$) from Eq. (12), while

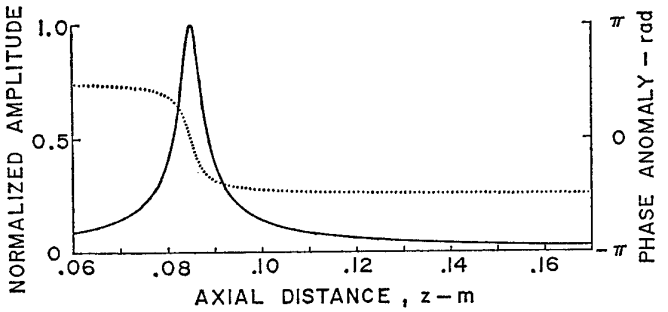

Fig. 2 Amplitude and phase anomaly of fundamental component on the axis.

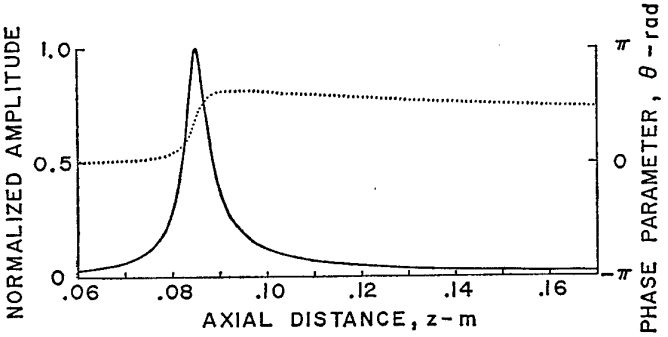

Fig. 3 Amplitude of second harmonic component and phase parameter on the axis.

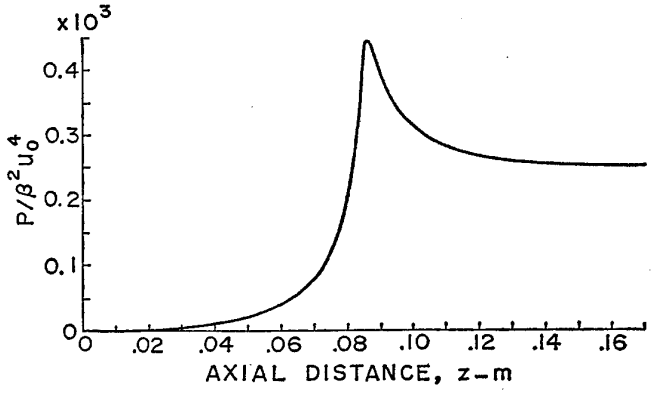

Fig. 4 Total power of second harmonic component passing through the plane perpendicular to the axis.

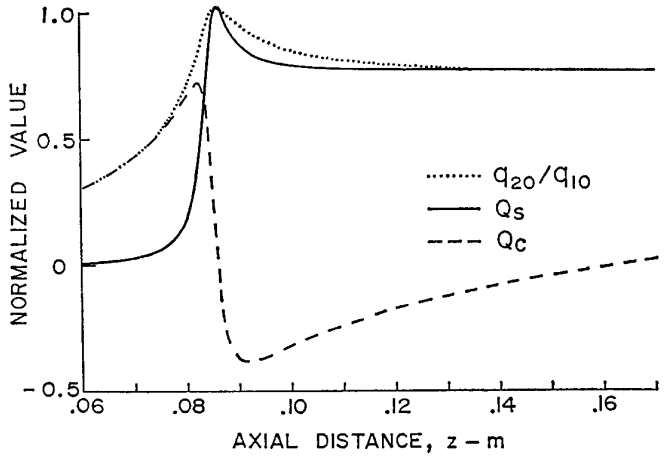

Fig. 5 The ratio q_{20}/q_{10} and its quadrature component Q_s $(=q_{20}/q_{10}\sin\theta)$ and in-phase component Q_c $(=q_{20}/q_{10}\cos\theta)$ along the axis.

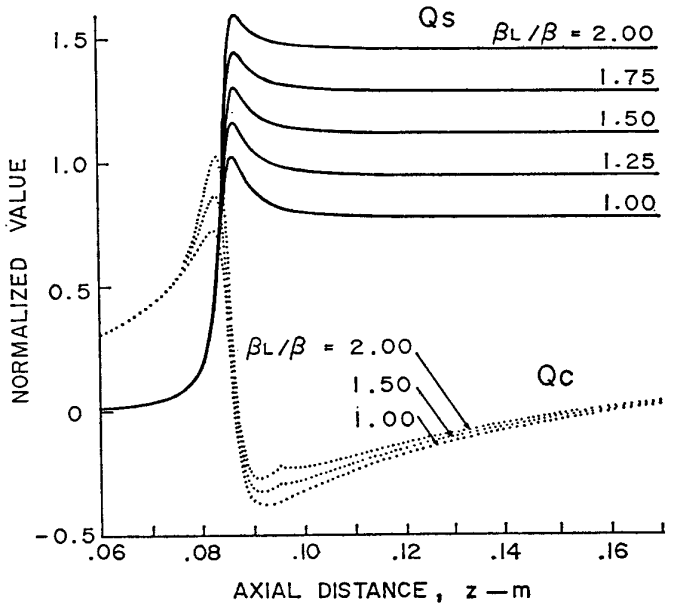

Fig. 6 The values of Q_s and Q_c along the axis with a sample of 20 mm thickness.

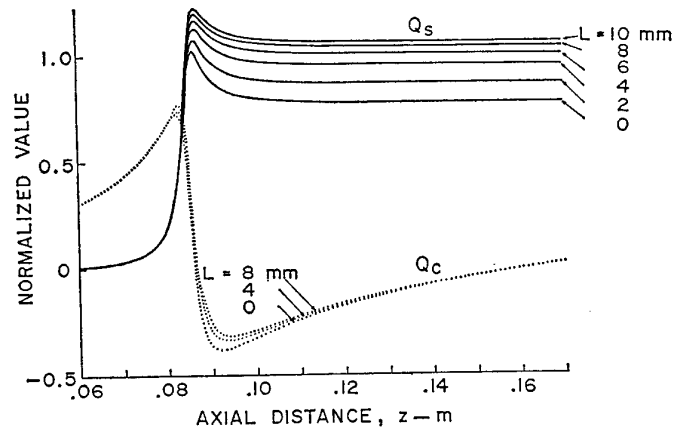

Fig. 7 The values of Q_s and Q_c along the axis with a sample with $\beta_L=1.5\,\beta$.

q_{20} is proportional to R^2 as expected in Eq. (16). Then the quantity q_{20}/q_{10} depends on $R^2/R=R$. In addition, the phase parameter $\theta_2-2\theta_1$ is independent of the r as seen from the same equations. Accordingly, an off-axis behavior of the values Q_s and Q_c can be easily predicted if those axial values are known. The computed axial values of q_{20}/q_{10}, Q_s and Q_c are shown in Fig. 5. In the pre-focal region, $Q_c=q_{20}/q_{10}$. However in the post focal region, the Q_c decreases and Q_s increases alternatively by a reason mentioned above. The sound pressure with large Q_c has the symmetry of the positive and negative portions of its waveform. A sawtooth wave, for example, should have large Q_c. On the other hand, the sound wave with large Q_s shows an asymmetrical form where crests are narrower than troughs. Such a waveform cannot be observed in non-diffracted sounds.

2.2 Influence of Inserted Sample

Let us suppose a condition where an infinitely broad sample is immersed into the focusing field normal to the acoustic axis. Here we assume that linear acoustic properties (ambient density and sound speed) are common to both the sample and surrounding water. Thus the second harmonic field is influenced by the sample. The fundamental component q_1 however remains unchanged as Eq. (12) shows. The changed value of q_2 can be easily obtained introducing new conditions for q_2 continuous at two sample-water boundaries.

For the case where a sample with thickness of $L=$ 20 mm is inserted within the range $D-L/2\leq z\leq D+L/2$ of the focal region, the axial values of Q_s and Q_c for various nonlinearity parameters of the sample β_L are shown in Fig. 6. While Q_s increases in proportion to β_L, the Q_c, which vanishes at $z=2D$, slightly changes according to the change of β_L. The axial values of Q_s and Q_c for various thickness L of the inserted sample with $\beta_L=1.5\,\beta$ are also shown in Fig. 7. Replacing the water with a sample within the range of 20% of the focal region length $\Delta z_{1/e}$ with its center at the focal plane, the Q_s increases more than 10% at $z=2D$. When the sample is as thick as the focal region, the value of Q_s tends to saturate.

3. EXPERIMENT

3.1 Experimental Arrangement

The block diagram of the experimental system is shown in Fig. 8. The arrangement is almost same as that in Ref. 14) excepting the sample and receiver. A cw pulse sound at 2.0 MHz emitted from a circular disk transducer with a radius of 40 mm was focused in degassed fresh water by a concave acoustic lens whose radius and focal length are 40 mm and 170 mm, respectively. The lens was fabricated from a high-density polyethylene slab, which has an absorption coefficient as high as 1.0 dB/mm at 2 MHz. Therefore the transmitted sound amplitude decreases as r increases on the lens, and the focusing effect is degraded. The source distribution was approximated by a Gaussian distribution for $A=720\ \mathrm{m}^{-2}$. In this case the focal region thickness $\Delta z_{1/e}$ is 40 mm.

Two kinds of receivers were employed in the experiment. One of them is a circular high-polymer piezofilm (Kynar piezofilm, product of Pennwalt corporation, USA) with thickness of 52 μm and radius of 13 mm, which has a square active element of 1 mm^2 area at the center. The receiving sensitivity is -127.4 ± 1.5 dB *re* 1 V/Pa in the range 1 MHz to 5 MHz. Another one is a spherical receiver of a 28 μm high-polymer piezofilm attached to an acryl slab with a concave curvature radius of 170 mm. By a use of this receiver centered perpendicularly on the acoustic axis at $z=2D=340$ mm as illustrated in Fig. 8, one can observe the sound in the manner similar to transmission type acoustical microscopes. A sensitivity was not calibrated for the latter receiver. Since this receiver is made of same piezofilm (Kynar piezofilm), a similar flat response as that of the former receiver can be expected.

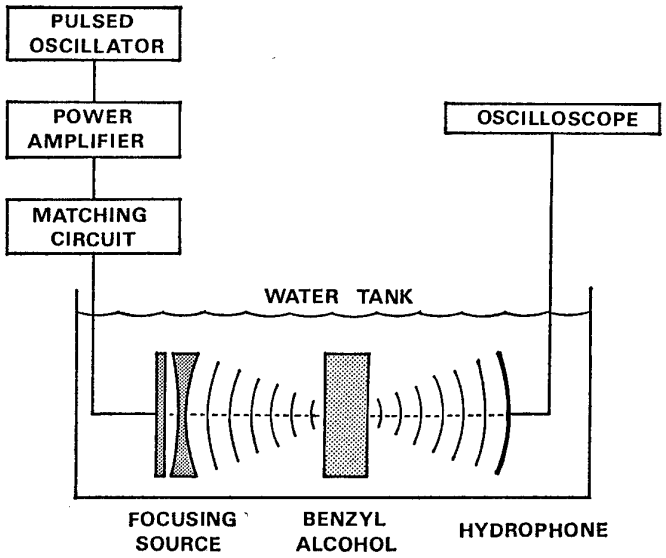

Fig. 8 Block diagram of experimental system.

Benzyl alcohol contained in the cavity, which has a window of rubber film as thin as 20 μm on each side, was employed for an inserting sample. The focusing beam propagates through the alcohol between two windows. At 20°C, the density, the sound speed and the nonlinearity parameter are 1,000 kg/m^3, 1,480 m/s and 3.5 in water, and 1,050 kg/m^3, 1,540 m/s and 6.1 in benzyl alcohol, respectively.[18] Therefore the assumption that only the parameter of nonlinearity of sample differs from the surrounding medium (water) is almost satisfied. Since the specific acoustic impedance of the rubber is close to that of water, the rubber film does not disturb the sound field. The sample thickness L is 30 mm, which is set by the dimension of the cavity.

The fundamental and second harmonic pressure at the focal point were 239.6 dB *re* 1 μPa and 227.5 dB *re* 1 μPa, respectively. Accordingly the ratio of the second harmonic amplitude to the fundamental amplitude is 0.25. This ratio corresponds to a shock parameter σ of 0.53 for the non-diffraction case and satisfies the quasilinear restriction ($\sigma<1$) to moderate amplitudes.

The wave profile of the received sound was observed on an oscilloscope and was simultaneously photographed. The waveform was quantized at 16 intervals over one period, and a Fourier transform was executed for a series of these data to obtain the amplitude ratio of the two harmonics and the phase parameter.

3.2 Experiment and Discussion

Since an experimental source radius is finite, the actual values of Q_s and Q_c may change rapidly with the position due to an edge diffraction. The fundamental component of this case can be given by Eq. (2) of Ref. 14),

$$q_1=-\frac{1}{z}\exp\left(j\frac{kr^2}{2z}\right)\int_0^a u(x)J_0\left(\frac{kr}{z}x\right)\cdot\exp\left\{j\frac{kx^2}{2}\left(\frac{1}{z}-\frac{1}{D}\right)\right\}xdx\,. \tag{20}$$

Modifying Eq. (7) of Ref. 14) one can obtain the second harmonic component observed at the back of the inserted sample ($z\geq z_L+L/2$, where z_L is the axial distance of the center of sample) as follows.

$$q_2=\frac{\beta k^2}{4\pi c_0 z}\exp\left(j\frac{kr^2}{z}\right)\int_{\xi=0}^{\pi}\int_{x=0}^{a}\int_{y=0}^{a}u(x)u(y)J_0\left(\frac{kr}{z}\sqrt{F}\right)$$
$$\times\left[\exp\left\{j\frac{k(x^2+y^2)}{2}\left(\frac{1}{z}-\frac{1}{D}\right)\right\}\exp(-jG)E_1(-jG)\right.$$
$$-\left(\frac{\beta_L}{\beta}-1\right)\exp\left\{j\frac{k(x^2+y^2)}{2}\left(\frac{1}{z_1}-\frac{1}{D}\right)+j\frac{kF}{4}\left(\frac{1}{z}-\frac{1}{z_1}\right)\right\}\exp(-jG_1)E_1(-jG_1)$$
$$\left.+\left(\frac{\beta_L}{\beta}-1\right)\exp\left\{j\frac{k(x^2+y^2)}{2}\left(\frac{1}{z_2}-\frac{1}{D}\right)+j\frac{kF}{4}\left(\frac{1}{z}-\frac{1}{z_2}\right)\right\}\exp(-jG_2)E_1(-jG_2)\right]xydydxd\xi\,, \qquad (21)$$

where

$$F=x^2+y^2-2xy\cos\xi\,,$$
$$z_1=z_L-L/2\,,$$
$$z_2=z_L+L/2\,,$$
$$G=k(x^2+y^2+2xy\cos\xi)/4z\,,$$
$$G_1=k(x^2+y^2+2xy\cos\xi)/4z_1\,,$$

and

$$G_2=k(x^2+y^2+2xy\cos\xi)/4z_2\,.$$

Here a is the source radius, $u(r)$ is the source velocity amplitude at the radial distance r, and $E_1(\cdot)$ is the exponential integral. Thus the values of Q_s and Q_c at any point beyond the sample can be obtained for the experimental source with the distribution $u(r)=u_0\exp(-720r^2)$ $(r\leq a)$ and $u=0$ $(r>a)$.

Table 1 compares the theoretical and experimental values of Q_s and Q_c at the point $z=270$ mm and $r=1.5$ mm when a benzyl alcohol sample with $L=30$ mm was put in three positions, $z_L=120$ mm, 170 mm and 220 mm. They are normalized so that the theoretical and experimental values of Q_s without sample are unity. The experimental shows a tendency similar to the theoretical. Putting alcohol sample within the focal region increases the experimental value Q_s by 44%; but with the sample placed at $z_L=120$ mm or 220 mm the magnitude of Q_s almost remains constant at the value measured in the case without any sample.

Table 1 Comparison of theoretical and experimental values of Q_s and Q_c for different sample positions.

z_L (mm)	Calculated		Measured	
	Q_s	Q_c	Q_s	Q_c
120	1.05	−0.10	1.05	−0.10
170	1.58	0.19	1.44	0.12
220	0.95	0.19	1.04	0.28

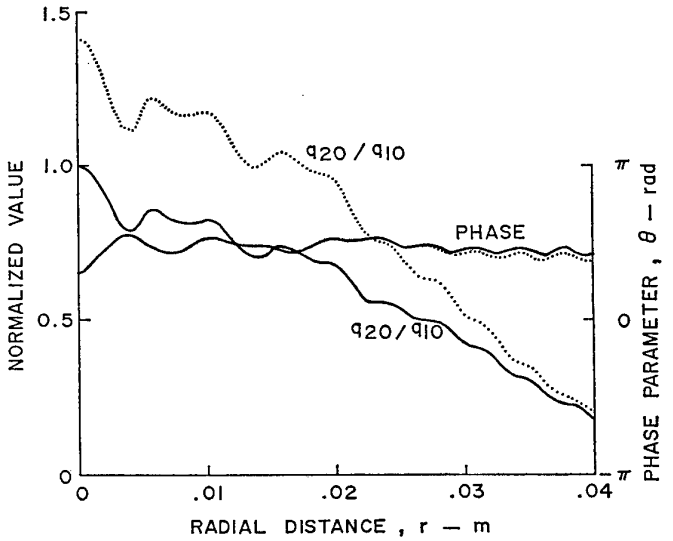

Fig. 9 Computed value of q_{20}/q_{10} and θ on sphere S; —— no sample, ····· sample with $\beta_L/\beta=1.5$ and $L=30$ mm.

When we suppose the situation is similar to transmission type microscopes, the detected sound pressure may become one averaged over the spherical receiver located at $z=2D-r^2/2D$. Two examples of the distributions of the amplitude ratio q_{20}/q_{10} and the phase parameter θ on the sphere S $(z=2D-r^2/2D)$ are shown in Fig. 9. The solid curves show the values for the case without inserted sample, and the dot curves show the values for the case with a sample inserted at the center of the focus, i.e. $z_L=D=170$ mm. The nonlinearity parameter and thickness of the sample are $1.5\,\beta$ and 30 mm, respectively. A sample with high nonlinearity makes the magnitude of the second harmonic component larger everywhere on the sphere. The value of θ is not much affected by the nonlinearity of samples.

Then the average values of Q_s and Q_c on the sphere S of the receiver can be also theoretically derived as

$$\left.\begin{aligned} \bar{Q}_s &= \left|\frac{\int \phi_2 dS}{\int \phi_1 dS}\right| \sin\bar{\theta} \\ \text{and} \\ \bar{Q}_c &= \left|\frac{\int \phi_2 dS}{\int \phi_1 dS}\right| \cos\bar{\theta}, \end{aligned}\right\} \quad (22)$$

where $\bar{\theta} = \angle \int \phi_2 dS - 2\angle \int \phi_1 dS$. Here $\int \cdot dS$ denotes the area integral on the sphere. The values of $\bar{Q}_s$ and $\bar{Q}_c$ affected by the sample inserted at the range $z_L = D = 170$ mm were numerically computed for the present experimental arrangement. Figure 10 shows $\bar{Q}_s$ and $\bar{Q}_c$ versus β_L of the samples with $L = 30$ mm and 60 mm. Figure 11 shows $\bar{Q}_s$ and $\bar{Q}_c$ versus L of the sample with $\beta_L = 1.5\,\beta$. It is obvious that the magnitude of $\bar{Q}_s$ grows with β_L and L, which reflects an intense virtual source of second harmonic sound in the focal region.

The distorted wave was observed by the spherical receiver when the sample of benzyl alcohol was inserted at each one of the three positions. Table 2 compares the values of $\bar{Q}_s$ and $\bar{Q}_c$ obtained through experiment with the respective values computed for $\beta_L/\beta = 1.74$. These values are similarly normalized so that both the experimental and theoretical values of $\bar{Q}_s$ without sample are unity as in Table 1. The experimental values show same tendency as the theoretical values. While $\bar{Q}_c$ increases without regard to the position of sample, $\bar{Q}_s$ changes only under the condition where the alcohol sample is placed in the focus. Therefore the $\bar{Q}_s$ is considered to be available for detecting the second harmonic component induced by the inserted sample.

If the experimental source is uniformly excited, i.e. $u(r) = u_0$, the thickness of the focal region reduces approximately to 70%, then the parameter of nonlinearity of thinner samples is presumably detected using $\bar{Q}_s$. A source with larger aperture angle to make a higher focusing gain and shorter focal region length would facilitate the application to thinner samples.

Reference 9) neglected the second harmonic sound generation in the pre-focal region and the important role played by the phase of the second harmonic sound. The present paper differs in that they have been taken into consideration.

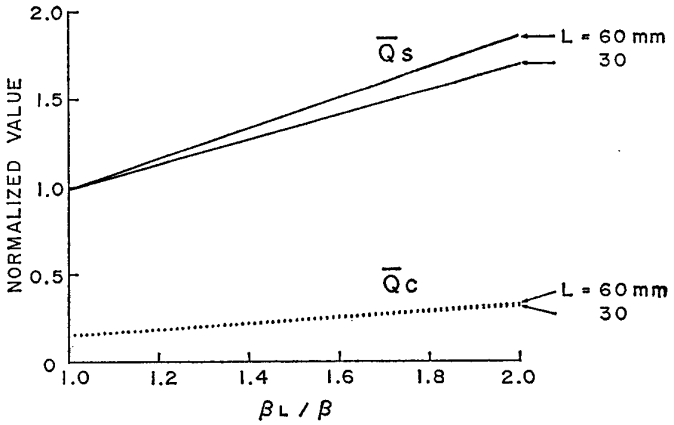

Fig. 10 Dependence of $\bar{Q}_s$ and $\bar{Q}_c$ on β_L of a sample with thickness of 30 mm or 60 mm.

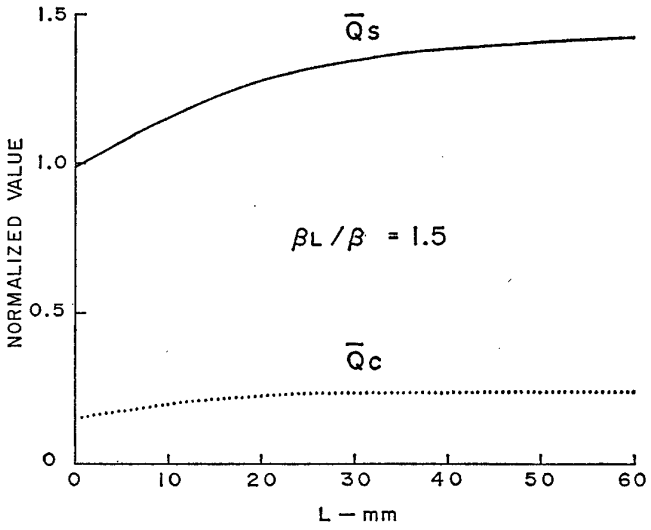

Fig. 11 Dependence of $\bar{Q}_s$ and $\bar{Q}_c$ on L of a sample with $\beta_L/\beta = 1.5$.

Table 2 Comparison of theoretical and experimental values of $\bar{Q}_s$ and $\bar{Q}_c$ for different sample positions.

z_L (mm)	Calculated		Measured	
	$\bar{Q}_s$	$\bar{Q}_c$	$\bar{Q}_s$	$\bar{Q}_c$
120	1.05	0.00	1.01	0.18
170	1.53	0.28	1.42	0.33
220	1.00	0.30	0.96	0.56

4. CONCLUSION

The present paper discussed the possibility of selective detection of the second harmonic component generated at the focal region to estimate the non-

linear property of the sample. The behavior of the second harmonic was theoretically predicted assuming a spherical focusing source whose excitation amplitude has a Gaussian distribution to avoid edge diffractions. A sample was assumed to have a parameter of nonlinearity different from that of the surrounding liquid (water). The influence of this sample on the second harmonic component, in particular the second harmonic detected by a spherical receiver arranged as in transmission type acoustical microscope, was examined theoretically and experimentally.

The result shows that the quadrature component which lags by $\pi/2$ radians compared to the second harmonic sound of non-diffraction case corresponds well to the component generated by the sample. On the other hand the inphase component is not much influenced by the sample. In the present computation for the case of a Gaussian source, if a sample with the parameter of nonlinearity 50% higher than that of water occupies 20% of the focal region length in thickness, the relative magnitude of the quadrature component $\bar{Q}_s$ increases by 10% or more. Accordingly it is possible to detect the nonlinear property of the inserted sample by the use of $\bar{Q}_s$.

Because relatively low frequency is employed, an absorption in water and benzyl alcohol sample is neglected here. The absorption coefficient is usually proportional to the frequency squared. If the source dimension becomes small in inverse proportion to a frequency, the effect of the absorption increases in proportion to the frequency. Therefore the absorption is not negligible at high frequencies. An unrealistic condition that the density and sound speed are common to both a sample and water is assumed in the present paper for simplicity. The sound absorption and the differences in density and sound speed would affect the intensity of the virtual source especially in the focal region and the destructive interference of the second harmonic in the post focal region.

ACKNOWLEDGMENTS

The authors wish to thank Prof. Minoru Nishimura of Tokai University for his encouragement. Dr. Thomas G. Muir of The University of Texas at Austin and the members of the Nonlinear Acoustics Research Society are thanked for their invaluable suggestions. The work was supported by a Grant-in-Aid for Scientific Research (#61550283), Ministry of Education.

REFERENCES

1) L. Bjørnø, "Aspects of nonlinear acoustics," in *Theoretical and Applied Mechanics*, ed. by F. I. Niordoson and N. Olhoff (Elsevier Science, New York, 1985), p. 97.
2) F. Dunn, "Nonlinear bioacoustics parameter," Proc. 12th ICA, Fl-1 (1986).
3) N. Ichida and T. Sato, "Nonlinear parameter tomography," J. Acoust. Soc. Jpn. (J) **39**, 521–530 (1983) (in Japanese).
4) N. Ichida, T. Sato, H. Miwa, and K. Murakami, "Real-time nonlinear parameter tomography using impulsive pumping waves," IEEE Trans. **SU-31**, 635–641 (1984).
5) I. Akiyama, M. Nakajima, and S. Yuta, "Proposal of nonlinearity parameter imaging by ultrasonic echo technique," Trans. IECE Jpn. **J68-C**, 588–589 (1985) (in Japanese).
6) C. A. Cain, "Ultrasonic reflection mode imaging of the nonlinear parameter B/A: I. A theoretical basis," J. Acoust. Soc. Am. **80**, 28–32 (1986).
7) T.G. Muir and E.L. Carstensen, "Prediction of nonlinear acoustic effects at biological frequencies and intensities," Ultrasound Med. Biol. **6**, 345–357(1980).
8) R. Kompfner and R. A. Lemons, "Nonlinear acoustic microscopy," Appl. Phys. Lett. **28**, 295–297(1976).
9) H. K. Wickramasinghe and C. Yeack, "Nonlinear imaging of an edge in the scanning acoustic microscope," J. Appl. Phys. **48**, 4951–4954 (1978).
10) C. E. Yeack, M.Chadorow, and C. C. Cutler, "Nonlinear acoustic off-axis imaging," J. Appl. Phys. **51**, 4631–4636 (1980).
11) M. R. T. Tan, H. L. Ransom, Jr., C. C. Cutler, and M. Chodorow, "Oblique, off-specular, linear, and nonlinear observations with a scanning micron wavelength acoustic microscope," J. Appl. Phys. **57**, 4931–4935 (1985).
12) B. G. Lucas and T. G. Muir, "The field of a focusing source," J. Acoust. Soc. Am. **72**, 1289–1296 (1982).
13) B. G. Lucas and T. G. Muir, "Field of a finite-amplitude focusing source," J. Acoust. Soc. Am. **74**, 1522–1528 (1983).
14) S. Saito, B. C. Kim, and T. G. Muir, "Second harmonic component of a nonlinearly distorted wave in a focused sound field," to be published in J. Acoust. Soc. Am.
15) V. F. Humphrey, M. Burgess, and N. Sampson, "Harmonic generation due to non-linear propagation in a focused ultrasonic field," Proc. Inst. Acoust. **8**, Conference on Ultrasound in Medicine, Bath Univ., 47–54 (1986).
16) D. Rugar, "Resolution beyond the diffraction limit in the acoustic microscope: A nonlinear effect," J. Appl. Phys. **56**, 1338–1346 (1984).
17) I.S. Gradshteyn and I. M. Ryzhik, *Table of Integrals, Series and Products* (Academic, New York, 1980).
18) R. T. Beyer, *Nonlinear Acoustics* (U.S. Naval Sea Systems Command, Washington, D.C., 1974), p. 101.